REGULAR *VERSUS* CHAOTIC DYNAMICS IN SYSTEMS GENERATED BY AREA-PRESERVING MAPS. APPLICATIONS TO THE STUDY OF SOME TRANSPORT PHENOMENA

DANA CONSTANTINESCU

Association Euratom-MEdC, Romania
University of Craiova, Department of Applied Mathematics,
13 A.I. Cuza Street, 200585 Craiova, Dolj, Romania
E-mail: dconsta@yahoo.com

Received September 21, 2015

In this paper we consider a class of discrete dynamical systems obtained through mapping technique from 3/2 d.o.f. Hamiltonian systems and we present some results concerning the existence and the position of internal transport barriers and a method for creating transport barriers in a prescribed position. Then we apply the results for mappings that model the magnetic field configuration in tokamaks and we interpret them.

Key words: plasma physics, transport phenomena, chaotic dynamics, area-preserving maps.

PACS: 52.25.Fi, 52.25. Xz, 52.25.Gj, 52.35.Vd.

1. INTRODUCTION

The study of discrete systems generated by area-preserving map is important both for theoretical and practical reasons. Different physical models analyzed already numerically and semi analytically concerning the diffusion of stochastic magnetic field lines [1]-[4], the zonal flow generation and pattern formation [5],[6], the diffusion of ions and electrons in stochastic electrostatic and magnetic fields in fusion plasma [7]-[10] can be analyzed also by the mapping technique. The approach based on the mapping technique was already used in the papers [11], [12] and based on fractional analysis in [13].

Many of them come from the discretization of 3/2 degrees of freedom Hamiltonian systems (*i.e.* 1 degree of freedom Hamiltonian systems subjected to a periodical time-dependent perturbation) and represent an efficient way to obtain information about the continuous system. This is important from practical point of view because 3/2 d.o.f. Hamiltonian systems, corresponding to specific Hamiltonians and interpretation of action-angle variables, are successfully used for the study of transport and mixing in the ocean and atmosphere [14],[15], of chaotic ray propagation in deep sea [16], of propagation of the pressure waves in pulsating stars of low mass [17], of magnetic configurations in hot plasma physics devices such as tokamaks [18]-[20].

These discrete systems are equally interesting from theoretical point of view because 3/2 d.o.f. Hamiltonian systems are generically non-integrable [18] and their main dynamical properties can be understood only through numerical discretization. There are two philosophically ways to obtain the discrete system associated to a 3/2 d.o.f. Hamiltonian system: using a symplectic numerical method with small step (for example symplectic Runge-Kutta method) or using mapping techniques with large step to construct a Poincaré map. We will focus on the discrete systems obtained through the mapping technique because it is very efficient and enables us to make some theoretical considerations and analytical proofs.

The typical picture of the phase for an area-preserving map reconstructs the properties of the continuous system. The non-perturbed case is integrable (the first integral is the Hamiltonian itself) and any orbit is periodic or quasiperiodic. In the perturbed case the situation is completely different. There are two types of periodic points: hyperbolic and elliptic. The elliptic ones are surrounded by invariant curves on which the orbits are quasiperiodic. For large enough perturbation, these "islands" of regular motion are surrounded by a "stochastic layer" [21] (called also stochastic sea or instability zone [22]) which contains the hyperbolic periodic points. The orbits of the points situated in this region are chaotic, *i.e.* they are decorrelated and exhibit sensitive dependence on initial conditions. The whole phase space is a complex structure of regular and chaotic zones which form fat fractals [23]. Both dynamical regimes are connected in a complicate layer where regular and chaotic motion can not mix. The complicate dynamics of the perturbed systems is partially due to the destruction of the invariant circles, which initially act as barriers. The permeability of the destroyed barrier enables the orbit to wander in a larger zone of the phase space.

The separation of the chaotic zones is very important in many phenomena: for transport and mixing in the ocean and atmosphere [24], these barriers may create some 'ozone holes' since they isolate the ozone created in the tropics from Earth's polar regions [14], [15], the chaotic ray propagation in deep sea and the propagation of the pressure waves in pulsating stars of low mass are also prevented by the existence of a transport barrier [16], [17]. In magnetic confinement fusion, the existence of internal transport barriers in the magnetic configurations of hot plasma physics devices, such as tokamaks, may be viewed as a fundamental prerequisite for the confinement of charged particles [18]. The partial destruction of the barriers explains the anomalous transport, which is observed in many phenomena.

In this paper we present some results about the existence and the position of transport barriers in systems generated by area-preserving maps. These results and the method for building transport barriers in a prescribed zone are exemplified using a realistic model for describing the magnetic field configuration in ASDEX-Upgrade tokamak.

The paper is structured as follows: in Section 2 are presented the main tools for

obtaining discrete systems associated to 3/2 d.o.f. Hamiltonian systems and theoretical results concerning the existence and the position of the transport barrier; Section 3 is devoted to the exemplification of the theoretical result using a realistic model for the description of the magnetic configuration in ASDEX-Upgrade; conclusions and discussions are given in Section 4.

2. TRANSPORT BARRIERS IN MAPPING MODELS

In what follows we will consider the Hamiltonian $H : S^1 \times D \times [0, \infty) \to \mathbf{R}$, written in action-angle variables (θ, I)

$$H(\theta, I, t) = H_0(I) + \varepsilon \cdot H_{pert}(\theta, I, t) \tag{1}$$

where S^1 denotes the circle $\mathbf{R}/(2\pi\mathbf{Z})$, $D \subset \mathbf{R}$ is the interval where the action variable I can vary and H_{pert} is periodic in time, with the main period T. Many techniques were considered for such systems, including quantization techniques in extended spaces [25]. The associated Hamiltonian system is

$$\begin{cases} \frac{\partial \theta}{\partial t} = H_0'(I) + \varepsilon \cdot \frac{\partial H_{pert}}{\partial I} \\ \frac{\partial I}{\partial t} = -\frac{\partial H_{pert}}{\partial \theta} \end{cases} \tag{2}$$

The essential dynamical aspects of such system are captured by the discrete dynamical system generated by the stroboscopic map with the stroboscopic time T, namely $SM_\varepsilon : S^1 \times D \to S^1 \times D$

$$SM_\varepsilon(\theta(0), I(0)) = (\theta(T), I(T))$$

It generates a two dimensional discrete dynamical system

$$(\theta_{n+1}, I_{n+1}) = SM_\varepsilon(\theta_n, I_n)$$

where $(\theta_n, I_n) = (\theta(nT), I(nT))$. The discrete orbit of $(\theta_0, I_0) = (\theta(0), I(0))$ is obtained by recording the coordinates of its trajectory at times T, $2T$, $3T$...

In [20] is shown that the stroboscopic map is a particular case of Poincaré map, adapted to the particular characteristics of 3/2 degrees of freedom Hamiltonian systems. In this way, the complex behavior of 3/2 degrees of freedom Hamiltonian systems can be understood by studying area preserving maps, which are relatively simpler mathematical objects than differential equations. The exact stroboscopic map can not be always analytically determined because this is equivalent to solving analytically the system. Usually it is approximated using various techniques, for example symplectic integrators or mapping techniques. The main goal of mapping models is to approximate the stroboscopic maps of the original system by symplectic maps obtained through Hamilton-Jacobi method [26]. They run much faster than the small step numerical integration, but the main advantage is that the mapping models

have better accuracy in the study of the chaotic dynamics due to the fact that the accumulation of the round-off errors is reduced.

The function $W(I) = H_0'(I)$, called winding (frequency) function, describes the rotation of the points in the unperturbed system and ε, called the stochasticity parameter, denotes the amplitude of the perturbation.

In the perturbed system, the rotation number of an initial condition (θ_0, I_0) is defined by [20]

$$R(\theta_0, I_0) = \lim_{n\to\infty} \frac{\theta_n - \theta_0}{n}.$$

For Hamiltonians with a 2π time-periodic perturbation

$$H(\theta, I, t) = H_0(I) + \varepsilon \sum_{m,n} H_{mn}(I) \cos(m\theta - nt)$$

it was proved [26] that the map $HJ_\varepsilon : S^1 \times \mathbf{R} \to S^1 \times \mathbf{R}$:

$$HJ_\varepsilon : \begin{cases} \overline{\theta} = \left(\theta + 2\pi \cdot W(X) + \varepsilon \frac{\partial S}{\partial X}(\theta, X, t) + \varepsilon \frac{\partial S}{\partial X}\left(\overline{\theta}, X, \overline{t}\right)\right) (\mathrm{mod}\, 2\pi) \\ \overline{I} = I - \varepsilon \frac{\partial S}{\partial \theta}(\theta, X, t) - \varepsilon \frac{\partial S}{\partial \overline{\theta}}\left(\overline{\theta}, X, \overline{t}\right) \end{cases} \tag{3}$$

is a very accurate approximation of the stroboscopic map. In eq. (3) X is the (unique) solution of the equation

$$X = I - \varepsilon \frac{\partial S}{\partial \theta}(\theta, X, t). \tag{4}$$

The generating function S, involved in (3),(4), is defined by [30]

$$S(\theta, X, t) = \frac{\pi}{k} \sum_{m,n} H_{mn}(I) \left[a(x_{mn}) \sin(m\theta - nt) + b(x_{mn}) \cos(m\theta - nt)\right] \tag{5}$$

where

$$a(x) = \frac{1 - \cos x}{x}; \qquad b(x) = \frac{\sin x}{x}, \quad x_{mn} = \frac{\pi}{k}(m \cdot W(X) - n). \tag{6}$$

In order to compute $HJ_\varepsilon(\theta, I, t)$ one must solve two (usually complicate) implicit equations: eq (4) and the first eq. in the system (3).

There are many interesting directions in the study of the system generated by the map (3), (4), but we focus on for the existence of internal transport barriers in models.

If W is a strictly non-degenerate monotonous function, *i.e.* $W'(I) \neq 0$ for all $I \in \mathbf{R}$, then (3), (4) is a twist map and one may apply the Kolmogorov-Arnold-Moser (KAM) theory in order to prove the existence of barriers and to explain their break-up [27]. In the reversed case, *i.e.* if there is a local extremum of W, it was observed that,

for small enough values of ε there is a robust barrier which intersects the shearless curve [28].

In [29] we analytically proved a general result concerning the existence of a robust barrier in systems (3), (4) with degenerate winding functions (reversed winding functions are particular cases):

Theorem 1: [13] Let $HJ_\varepsilon : S^1 \times [a,b] \to S^1 \times [a,b]$ be the map (3), (4). If $H_{mn}(a) = 0$ for all m, n and there is $I_0 \in [a,b]$ such that $W'(I_0) = 0$, then, for small enough values of ε, the map HJ_ε has infinitely many invariant rotational circles with the rotation number close to $W(I_0)$. They form a transport barrier which intersects the degenerate curve

$$C_{\deg,\varepsilon} : I = I_0 + \varepsilon \frac{\partial S}{\partial \theta}(\theta, I_0)$$

This result enabled us to propose a method for creating internal transport barriers in twist systems [30]. It is sufficient to modify locally the winding function without affecting its monotony and to create a zone where W is flat, *i.e.* there is I_0 such that $W'(I_0) = 0$.

A possible controlled winding function W_c may depend on three values of I, namely $I_1 < I_0 < I_2$ and it could have the following properties:

- W_c coincides with W outside the interval $[I_1, I_2]$;
- W_c is derivable in I_1 and I_2;
- $W_c'(I_0) = 0$;
-W_c is a monotonous function;

In [30] it was found that a candidate satisfying these criteria is given by

$$W_c(I) = \begin{cases} W(I) & \text{if } I \notin [I_1, I_2] \\ W_0 - c_1 (I - I_0)^7 - c_2 (I - I_0)^5 - c_3 (I - I_0)^3 & \text{if } I_1 \le I \le I_2 \end{cases} \tag{7}$$

where the parameters W_0, c_1, c_2, c_3 are computed using the continuity and the derivability of W_c in I_1 and I_2 (four conditions).

The efficiency of this method was already proved in [29], [30] using mapping models with a small number of terms (less than 10) in the Hamiltonian perturbation. In the following Section we will apply it for a model with 1880 MHD modes active in the same time. This model is important in the study of magnetic field's configuration in tokamaks.

3. THE MAGNETIC MODEL

In models for describing phenomena that occur in tokamaks the toroidal coordinates (r, θ, ζ) are commonly used because the tokamaks are toroidal devices: ζ is the toroidal angle and (r, θ) are the poloidal coordinates in a circular poloidal section. When the model study the magnetic configuration the poloidal radius r is replaced

by the toroidal flux $\psi = r^2/2$ because ψ and θ represent a pair of canonical variables [19].

The configurations of the magnetic field may be modeled using Hamiltonian description [20].

The Hamiltonian is obtained from the equations of the magnetic field using the Clebsh representation. It is in fact the poloidal magnetic flux

$$H(\theta, \psi, \zeta) = H_0(\psi) + \varepsilon \cdot H_{pert}(\theta, \psi, \zeta).$$

The unperturbed Hamiltonian, $H_0(\psi) = \int \frac{d\psi}{q(\psi)} = \int W(\psi)\, d\psi$, is the poloidal flux of the equilibrium plasma.
The effect of magnetic perturbations (generated by coil imperfections as well as internal instabilities [12]) is contained in the term $\varepsilon \cdot H_{pert}(\theta, \psi, \zeta)$.

In this case ψ represent the action variable and the toroidal angle ζ is interpreted in analogy with a "time variable".

The "time" section, $(S) : \zeta = \zeta_0$ is a vertical poloidal section of the device, *i.e.* $(S) = S^1 \times [0, \infty)$. The physical relevant interval for ψ is $[0, 1]$.

In this case, the mapping models (3), (4) have an important physical interpretation: the pair (θ_n, ψ_n) indicates the re-intersection of the magnetic field line starting from (θ_0, ψ_0) with (S) after toroidal n turns.

Many mapping models that are in qualitative agreement with experimental observations were already proposed and studied, see [18], [26], [33] and the references therein. All these models consider perturbations with a small numbers of locked MHD modes, due to high difficulty in implementing the mapping technique. They represent an important step in understanding the behavior of the continuous system (which is much more difficult to study through classical numerical methods, for example symplectic Runge-Kutta) but they have a drawback for experimentalists: the chaotic behavior is obtained for quite large amplitude of perturbations, which is not in agreement with the situation encountered in real devices ($\varepsilon < 10^{-2}$). This deficiency is eliminated if one considers a large number of locked MHD modes, as in our study.

The magnetic field is determined by the safety factor and the magnetic perturbations. The determination of these quantities from experiments is a challenging task, due to the large uncertainties in the measurements.

The safety factor $q(r)$ is determined by the radial distribution of the plasma current density. In experiments the safety factor can be derived from the observation of large striations identified during the ablation of injected hydrogen (deuterium) pellets [31].

It can be analytically obtained from the magneto-hydrodynamic theory [32], or from equilibrium code calculations, taking into account the position of the MHD modes identified in experiments [36].

In our examples we will use the safety factor used in [36], namely

$$q(\psi) = 0.8 + 4\psi; \tag{8}$$

The magnetic perturbations are due to plasma instabilities (MHD-perturbations) or the addition of internal or external magnetic fields usually created by external applied electric currents (RMP-perturbations). The MHD-perturbations (magneto-hydrodynamic perturbations) corresponding to the (m,n) mode reads

$$H_{mn}(\psi)\cos(m\theta - n\zeta + \chi_{mn})$$

where m,n are the poloidal and toroidal number and χ_{mn} is the mode's phase. The winding number of the (m,n) mode in the unperturbed system is $W(\psi_{mn}) = n/m$, *i.e.* $q(\psi_{mn}) = m/n$. It means that the mode (m,n) is resonant at magnetic surface $\psi = \psi_{mn}$.

In what follows we will use the MHD-perturbation proposed in [33]:

$$H_{mn} = \frac{n}{m}\left[\frac{(\psi/\psi_{mn})^{1/\Delta} + (\psi/\psi_{mn})^{-1/\Delta}}{2}\right]^{-m\Delta/2}. \tag{9}$$

The profile of MHD mode correctly describes the behavior near the resonant surfaces and it is in agreement with the parametrization proposed in [34], [35]

The internal magnetic perturbations which contains several (m,n) modes is

$$\varepsilon \cdot H_{pert}(\theta,\psi,\zeta) = \sum_{m,n} H_{mn}(\psi)\cos(m\theta - n\zeta)$$

The model we analyze the perturbation H_{pert} contains all (m,n) modes with $1 \le m \le 40$, $\frac{1}{4} < \frac{m}{n} < 1$ (*i.e.* 1880 terms in the sum).

The main problem we encountered was a computational one, because very complicate implicit equations must be solved for each $n \in \mathbf{N}$ in order to pass from (θ_n, ψ_n) to $(\theta_{n+1}, \psi_{n+1})$. In this case the efficiency of the mapping method is effective because much numerous similar equations should have been solved in symplectic Runge-Kutta method for obtaining the same result.

The numerical simulations were performed using a FORTRAN code especially designed for this purpose.

It was observed that, even for very small values ($\varepsilon = 10^{-5}$), the chaotic behavior appears. The phase portrait practically reproduces the results obtained from gyrokinetic simulations [38]. This proves that the model is a realistic one.

In all numerical simulations we considered $\varepsilon = 10^{-5}$ and $\Delta = 0.01$.

In Figure 1 the variation of ψ along the orbits of $(\theta_0, \psi_0) = (5.2025, 0.0103)$ (blue) and $(\theta_1, \psi_1) = (5.1880, 0.01192)$ (green) is presented. We considered long orbits $N = 10^5$.

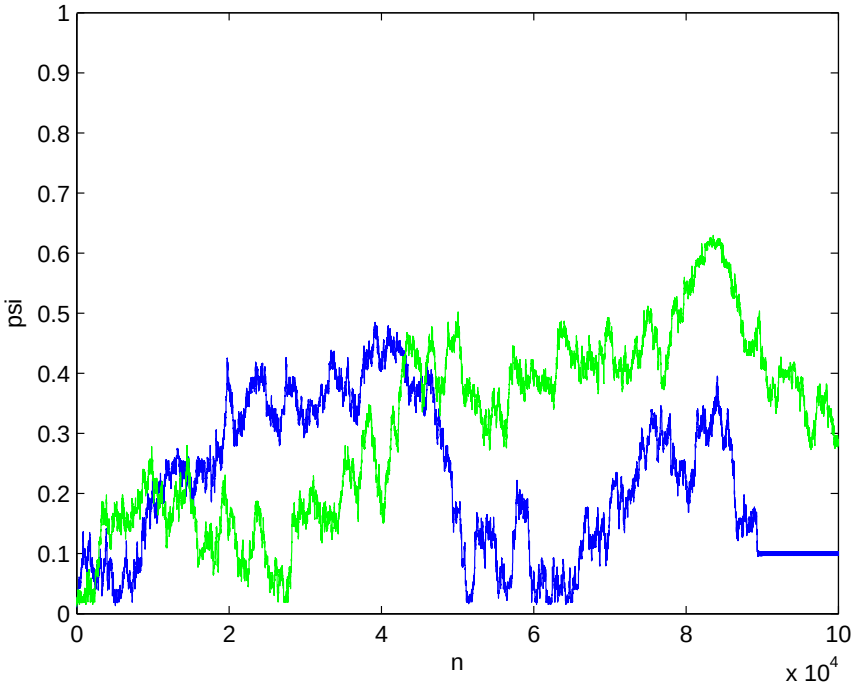

Fig. 1 – (Color on-line). The variation of ψ in the orbit of $(\theta_0, \psi_0) = (5.2025, 0.0103)$ (blue) and $(\theta_1, \psi_1) = (5.1880, 0.01192)$ (green) in the original system.

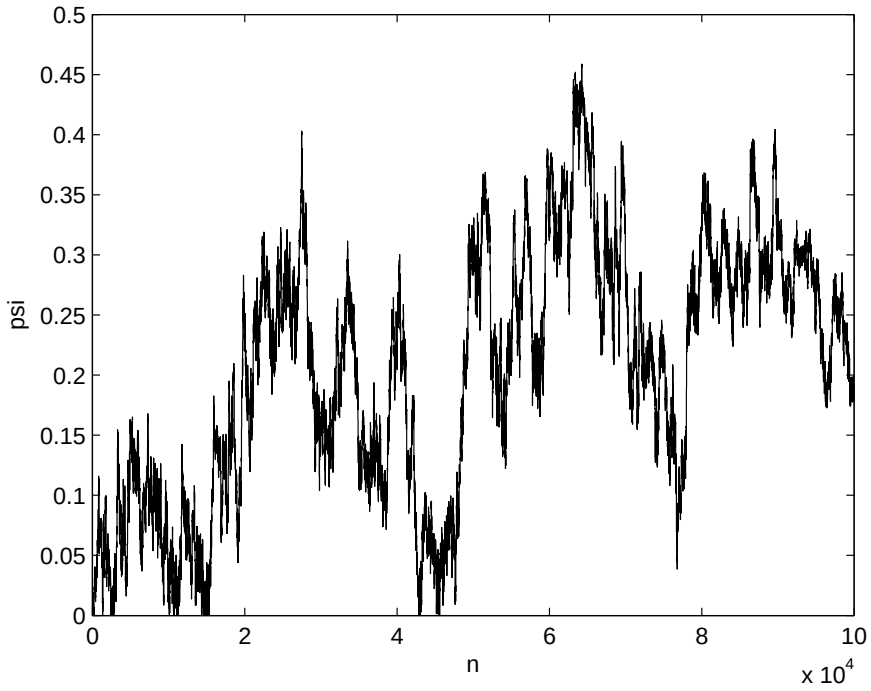

Fig. 2 – (Color on-line). The values of $|\psi_1(n) - \psi_0(n)|$ for the orbits presented in Figure 1. It shows that the system exhibits sensitive dependence on initial conditions because $|\psi_1(n) - \psi_0(n)| > 0.15$ for $n > 8 \cdot 10^4$.

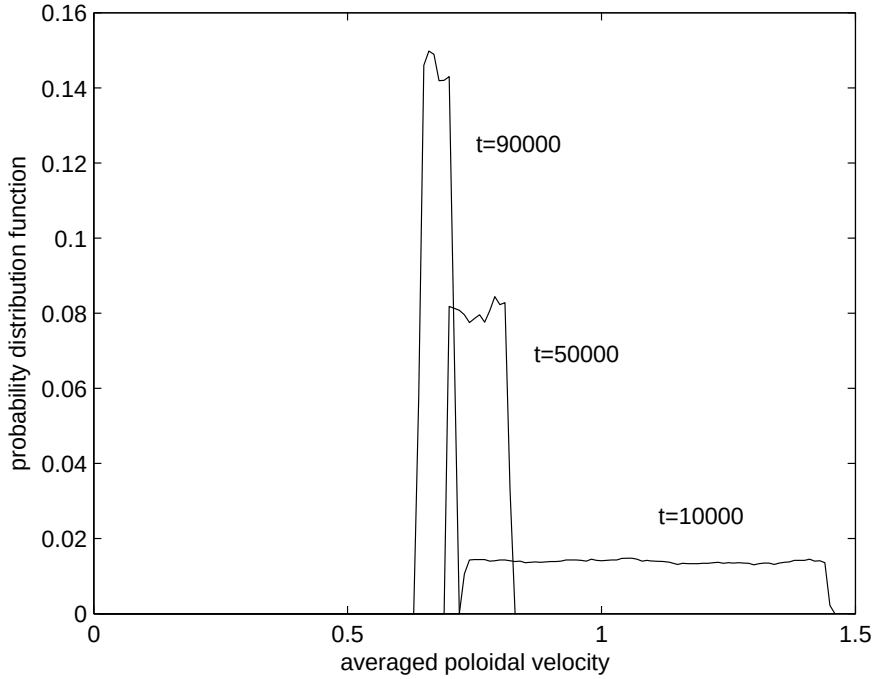

Fig. 3 – (Color on-line). The probability distribution function of the poloidal velocity over the first 10 000 points on the orbit of (θ_1, ψ_1).

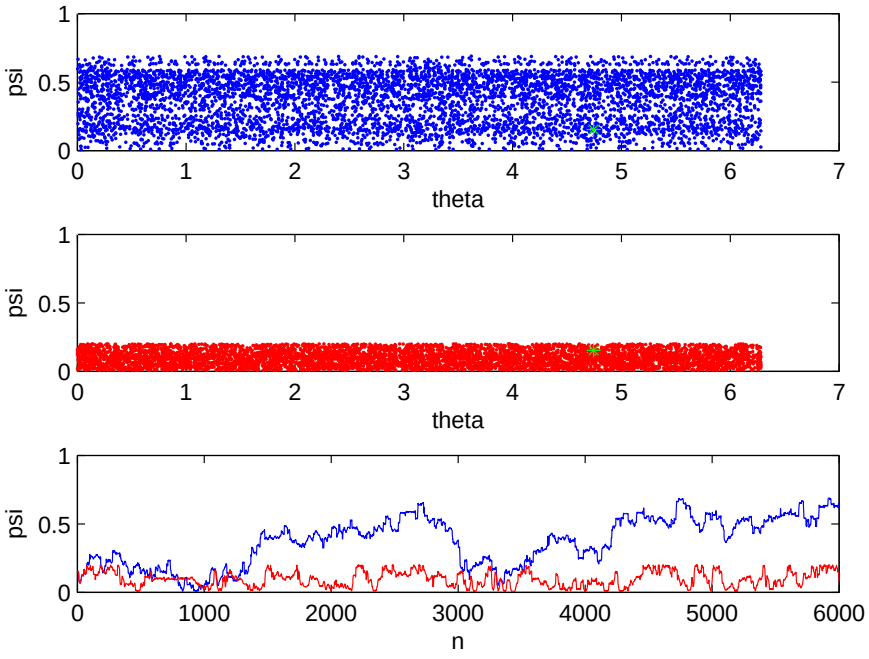

Fig. 4 – (Color on-line). The orbit of $(\theta, \psi) = (4.7441, 0.1529)$ in blue is the orgininal one, in red is the controlled one ($\psi_1 = 0.2$, $\psi_0 = 0.3$, $\psi_2 = 0.4$)

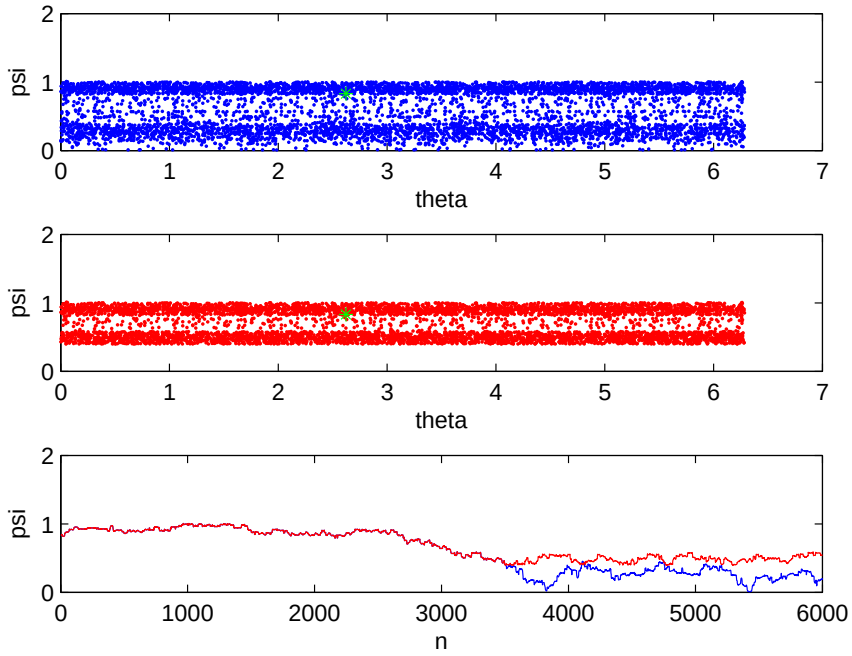

Fig. 5 – (Color on-line). The orbit of $(\theta, \psi) = (2.6212, 0.8294)$ in blue is the orgininal one, in red is the controlled one ($\psi_1 = 0.2$, $\psi_0 = 0.3$, $\psi_2 = 0.4$)

In the green orbit one can observe a sticking phenomena between the islands chains (9,4) and (8,3), as long as $\psi_{9,4} = 0.3625 < \psi < \psi_{8,3} = 0.4667$. The blue orbit is captured by a an island chain of order II situated around the island chain of type (4,3).

Figure 2 presents the differences $|\psi_1(n) - \psi_0(n)|$, $n \in \{1, 2, ...10^5\}$ for the orbits presented in Figure 1. Because the initial points of the orbits are close, *i.e.* $d((\theta_0, \psi_0), (\theta_1, \psi_1)) = 0.0146$, the fact that $|\psi_1(n) - \psi_0(n)| > 0.2$ for $n > 8 \cdot 10^4$ can be considered a sign of sensitive dependence on initial conditions. It may be considered that the orbits are chaotic.

In Figure 3 is presented the probability distribution function of the poloidal velocity over the first 10 000 points on the orbit of (θ_1, ψ_1), which are uniformly spread in the whole chaotic zone occupied by the orbit. The figure show a ratchet-like transport in the poloidal direction [37].

In order to observe if the controlled winding function (7) generates a transport barrier, we considered in (7) $\psi_1 = 0.2$, $\psi_0 = 0.3$, $\psi_2 = 0.4$.

Figure 4 presents the orbit of $(\theta, \psi) = (4.7441, 0.1529)$ in the original system (blue) and in the controlled one (red). The initial data is situated under the built barrier. The orbit of the original system walks in the whole phase space and the controlled orbit do not cross the barrier (the red orbit remains in the lower zone of the figure).

The same phenomenon can be observed in Figure 5, where the original and the controlled orbit of $(\theta, \psi) = (2.6212, 0.8294)$ are presented. The blue orbit is the original one, in red orbit is the controlled one. In the beginning, before entering in the controlled zone, the orbits coincide. After this, the controlled orbit remains above the barrier and does not cross it.

The transport barriers surrounds the invariant circle $\psi_0 = 0.3$, which is in agreement with the theoretical results [13].

It becomes evident that the modification of the winding function, implicitly of the safety factor, is a key method in obtaining transport barriers.

4. CONCLUSIONS

In this paper some results about systems generated by area-preserving maps were presented. We developed a model for magnetic lines, in which the situation is analogous to that occurring in toroidal plasmas in the ideal case (no magnetic drifts, no electric field, no collisions). The results of the numerical simulations are in agreement with the results obtained from gyrokinetic simulations, which proves that the model we propose captures the main features of the magnetic configuration.

Of course, the internal transport barriers observed in experiments have not purely magnetic origin, as in the model studied here, but the magnetic transport barri-

ers inhibit radial transport of heat and particles which predominantly follow magnetic lines. For this reason, the method we propose for creating magnetic transport barriers is interesting for improving the plasma confinement in tokamaks.

Acknowledgements. This work has been carried out within the framework of the EUROfusion Consortium and has received funding from the Euratom research and training programme 2014-2018 under grant agreement No 633053. The views and opinions expressed herein do not necessarily reflect those of the European Commission.

REFERENCES

1. M. Negrea, I. Petrisor, R. Balescu, Phys. Rev. E **70**, 046409 (2004).
2. M. Negrea, I. Petrisor, Physics AUC **16** (part. 1), 28–43 (2006).
3. M. Negrea, I. Petrisor, B. Weyssow, Plasma Phys. Control. Fusion **49**, 1767–1781 (2007).
4. Gy. Steinbrecher, M. Negrea, N. Pometescu, J. H. Misguich, Plasma Phys. Control. Fusion **39**, 2039–2049 (1997).
5. R. Balescu, M. Negrea, I. Petrisor, Plasma Phys. Control. Fusion **47**, 2145–2159 (2005).
6. M. Negrea, I. Petrisor, B. Weyssow, Phys. Scr. **77**, 055502 (2008).
7. I. Petrisor, M. Negrea, Physics AUC **22**, 68–76 (2012).
8. I. Petrisor, M. Negrea, B. Weyssow, Phys. Scr. **75**, 1 (2007).
9. M. Negrea, I. Petrisor, B. Weyssow, J. Optoelectron. Adv. M. **10**, 1942–1945 (2008).
10. M. Negrea, I. Petrisor, D. Constantinescu, Rom. J. Phys. **55**, 1013–1023 (2010).
11. D. Constantinescu, M. Negrea, I. Petrisor, Rom. J. Phys. **55**, 951–960 (2010).
12. D. Constantinescu, M. Negrea, I. Petrisor, Physics AUC **24**, 123–129 (2014).
13. D. Constantinescu, M. Negrea, I. Petrisor, Physics AUC **24**, 104–115 (2014).
14. D. Del Castillo-Negrete, P. J. Morrison, Phys. Fluid A **5**, 948–965 (1993).
15. I. Rypina, M. G. Brown, F. J. Beron-Vera, H. Kocak, M. J. Olascoaga, I. Udovydchenkov, J. Atmos. Sci. **64**, 3595–3610 (2007).
16. I. P. Smirnov, A. L. Virovlyansky, G. M. Zaslavsky, Phys. Rev. E **64**, 036221 (2001).
17. A. Munteanu, E. Petrisor, E. Garcia-Berro, J. Jose, Commun. Nonlinear Sci. Numer. Simul. **8**, 355–373 (2003).
18. R. Balescu, Phys. Rev. E **58**, 3781–3792 (1998).
19. R. Balescu, M. Vlad, F. Spineanu, Phys. Rev. E **58**, 951–964 (1998).
20. P. J. Morrison, Phys. Plasmas **7**, 2279–2289 (2000).
21. S. S. Abdullaev, Phys. Rev. E **62**, 3508–3527 (2000).
22. V. Afraimovich, A. Maass, J. Urias, Nonlinearity **3**, 617–637 (2000).
23. R. Eykholt, D. K. Umberger, Phys. Rev. Lett. **57**, 2333–2337 (1986).
24. R. Cimpoiasu, R. Constantinescu, Cent. Eur. J. Phys. **12**, 81–89 (2014).
25. R. Constantinescu, J. Math. Phys. **38**, 2786–2794 (1997).
26. S. S. Abdulaev, Nucl. Fusion **44**, S12–S27 (2004).
27. R. S. MacKay, "*Renormalization in Area-Preserving Maps*" (Advanced Series in Nonlinear Dynamics, World Scientific, Singapore, 1993).
28. A. Delshams, R. de la Llave, SIAM J. Math. Anal. **31**, 1235–1269 (2000).
29. D. Constantinescu, M.-C. Firpo, Int. J. Bifurcat. Chaos **23**, 1350034 (2013).
30. D. Constantinescu, M.-C. Firpo, Nucl. Fusion **52**, 054006 (2012).

31. M. A. Dubois, S. Sabot, B. Pegourie, H.-W. Drawin, A. Geraud, Nucl. Fusion **32**, 1935–1940 (1992).
32. J. H. Misguich, J. D. Reuss, B. Weysow, D. Constantinescu, G. Steinbrecher, R. Balescu, M. Vlad, F. Spineanu, Annales de Physique **28**, 1–101 (2003).
33. S. S. Abdullaev, Nucl. Fusion **50**, 034001 (2010).
34. J. P. Meskat, H. Zohm, G. Gantenbein, S. Gunter, M. Maraschek, W. Suttrop, Q. Yu and the ASDEX Upgrade Team, Plasma Phys. Contr. Fusion **43**, 1325–1332 (2001).
35. V. Igochine, O. Dumbrajs, D. Constantinescu, H. Zohm, G. Zvejnieks and the SDEX Upgrade Team, Nucl. Fusion **46**, 741–751 (2006).
36. O. Dumbrajs, V. Igochine, D. Constantinescu, H. Zohm, Phys. Plasmas **12**, 110704 (2005).
37. A. B. Schelin, K. H. Spatschek, Phys. Rev. E **81**, 016205 (2010).
38. H. Doerk, F. Jenko, M. J. Pueschel, D. R. Hatch, Phys. Rev. Lett. **106**, 155003 (2011).